

Strain-driven valley states and phase transitions in Janus VSiGeN₄ monolayer

Pengyu Liu,¹ Siyuan Liu,¹ Minglei Jia,¹ Huabing Yin,¹ Guangbiao Zhang,¹ Fengzhu Ren,^{1,*} Bing Wang,^{1,†} and Chang Liu^{1,‡}

¹*Institute for Computational Materials Science, Joint Center for Theoretical Physics (JCTP),
School of Physics and Electronics, Henan University, Kaifeng, 475004, China*

(Dated: June 3, 2022)

The interplay between topology and valley degree of freedom has attracted much interest because it can realize new phenomena and applications. Here, based on first-principles calculations, we demonstrate intrinsically valley-polarized quantum anomalous Hall effect in monolayer ferrovalley material: Janus VSiGeN₄, of which the edge states are chiral-spin-valley locking. Besides, a small tensile or compressive strain can drive phase transition in the material from valley-polarized quantum anomalous Hall state to half-valley-metal state. With the increase of the strain, the material turns into ferrovalley semiconductor with valley anomalous Hall effect. The origin of phase transition is sequent band inversion of V d orbital at K valley. Moreover, we find that phase transition causes the sign reversal of Berry curvature and induces different polarized light absorption in different valley states. Our work provides an ideal material platform for practical applications and experimental exploration of the interplay between topology, spintronics, and valleytronics.

I. INTRODUCTION

The valley, local maximum or local minimum of electronic band structure in momentum space, provides valley degree of freedom to encode and manipulate information analogous to charge and spin [1–3], the related field is called valleytronics. For utilizing the valley index as an information carrier, the key is how to break the energy degeneracy of the valley in the valleytronics material, which can create carries imbalance between different valleys to be detected [4]. The experimental discovery of two-dimensional (2D) transition metal dichalcogenides (TMDs) has greatly promoted the development of valleytronics [5–17]. It is found that optical pumping can produce valley polarization in MoS₂ based on the valley-contrasting optical selection rules [6, 7], a finding that can be applied to valley optoelectronic devices [18, 19]. Unfortunately, due to the short lifetime of the carries, the valley will depolarize quickly and cause information loss. On the other hand, some experiments reported that Zeeman effect of external magnetic field can break the energy degeneracy of valleys in TMD [11, 12]. However, the efficiency of magnetic field is low (0.1 ~ 0.2 meV/T), thereby it is difficult to preserve a suitable valley splitting value by magnetic field in electronic equipment. Besides, it was found that magnetic doping and magnetic proximity effect can induce valley polarization [20–22]. Especially, a larger than 300 meV valley splitting in MoTe₂ can be induced by magnetic substrate of EuO [23]. Yet, the magnetic substrate submerges the valley physics of host materials, and magnetic doping usually increases impurity scatterings between different valleys. Valley polarization induced by above ways is volatile. Thus, it is important to find intrinsic valley polarization.

Recently, valleytronic material have been extended to 2D ferromagnetic system named ferrovalley [24–37]. When both time-reversal and inversion symmetry are broken, ferrovalley materials can produce spontaneous valley polarization and

realize anomalous valley Hall effect (AVHE) [24, 27], and these properties can be well applied to data process or data storage. Importantly, out-of-plane magnetization is a necessary condition for achieving spontaneous valley polarization [29, 33, 38]. However, most of the discovered ferrovalley materials have in-plane magnetization [28, 29, 31, 39], and thus require difficult modulation of the magnetic easy axis. On the other hand, some novel quantum states were discovered in ferrovalley materials, such as topological state and half-valley-metal (HVM) state [32, 35]. The multiple valley states not only enrich valley degree of freedom and quantum states but also bring intriguing physical properties, such as valley-polarized quantum anomalous effect (VQAHE) and selective absorption of polarized light [25, 34, 35]. Though highly valuable, ferrovalley material with both modulate multiple valley states and out-of-plane magnetization is quite rare.

In this work, we predict a ferrovalley material of Janus VSiGeN₄ monolayer based on density-functional theory (DFT). We find that this monolayer can not only maintain valley characteristics, but also has large valley polarization and strain-induced phase transition. Our results show that monolayer VSiGeN₄ is a ferromagnetic semiconductor, and it has out-of-plane magnetization with a Curie temperature of 113K. Interestingly, the material possesses a VQAHE with chiral-spin-valley locking edge states. Besides, it becomes HVM with 100% valley polarization under tiny tensile strain of 0.1% or compressive strain of 0.32%. By continuing to increase the strain, the material will transform into ferrovalley semiconductor (FVS), which shows an AVHE. Moreover, the polarized light absorption and the sign of berry curvature located in the K+ and K− valley can also be modulated by applying strain. Our work thus enriches materials with valley-related multiple Hall effect and provides a platform for research valleytronics, spintronics, and topology.

II. COMPUTATIONAL METHODS

All the first-principles calculations were performed using the projector-augmented wave (PAW) method [40], which is embedded in the Vienna *ab initio* Simulation Package (VASP)

* f.z.ren@henu.edu.cn

† wb@henu.edu.cn

‡ cliu@vip.henu.edu.cn

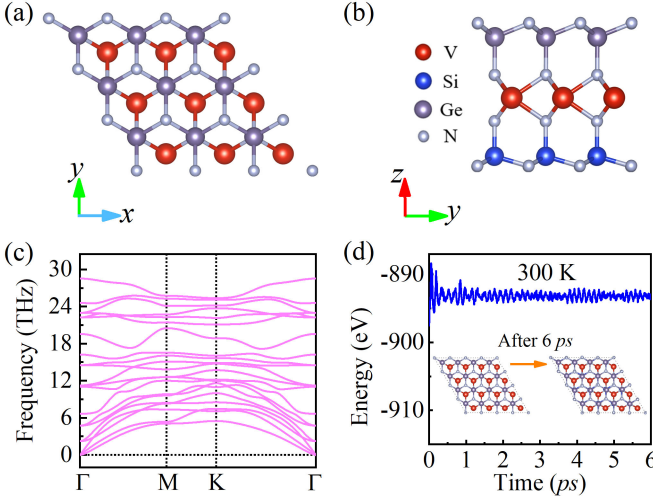


FIG. 1. (a) and (b) Top and side views of ML VSiGeN₄, respectively. (c) Phonon dispersion spectrum and (d) energy variation during the 6 ps AIMD simulation at 300K. Insets in (d) display the initial and final structures of ML VSiGeN₄ in the MD simulation.

[41]. The exchange and correlation interaction is described by the Perdew-Burke-Ernzerhof (PBE) functional with the general gradient approximation (GGA) [42]. The spin-orbit coupling (SOC) effect is included in the calculations. We use Γ -centered k -meshes of $15 \times 15 \times 1$ for the Brillouin-zone (BZ) sampling and 500 eV cutoff energy for the plane wave basis. The convergence criterion for energy and force is chosen as 10^{-6} eV and 0.01 eV/Å, respectively. A vacuum region of 20 Å is taken to eliminate the interactions between periodic layers. The GGA+U method is adopted to describe the strong correlated correction of V-3d orbitals and the U parameter is chosen as 3 eV [25, 28, 37]. The *ab initio* molecular dynamic (AIMD) simulation is performed by using a $4 \times 4 \times 1$ supercell to determine thermal stability. Phonon spectrum is calculated by using the density functional perturbation theory (DFPT) with a $4 \times 4 \times 1$ supercell. The edge states and Chern number were calculated by using the WANNIER90 package [43] and WANNIERTOOLS package [44]. The Monte Carlo (MC) simulations are performed on a 2D 16×16 supercell based on the standard Metropolis-Hasting algorithm, and we use 640000 sweeps to get reasonable result.

III. STRUCTURE STABILITIES AND MAGNETISM

The Janus monolayer (ML) VSiGeN₄ has a triangular lattice structure with space group P3M1, and the optimized lattice constant is $a = b = 2.96$ Å. As shown in Fig. 1(a) and Fig. 1(b), the lattice has no space inversion symmetry, and the structure is built up by septuple atomic layers in the sequence of N-Ge-N-V-N-Si-N, which can be viewed as VN₂ layer sandwiched by a Ge-N and Si-N layer. To confirm the stability of structure, the phonon spectra and molecular dynamic (MD) simulation are shown in Fig. 1(c) and Fig. 1(d), respectively. The absence of imaginary frequencies in phonon

spectra confirms the dynamics stability. After 6 ps MD simulation at 300K, no destruction is observed in ML VSiGeN₄, which indicates the thermal stability under 300K. Besides, we calculated the formation energy of ML VSiGeN₄: $E_f = (E_{total} - E_{Si} - E_V - E_{Ge} - 4E_N)/n$. Where E_{total} represent the total energy of ML VSiGeN₄ in the primitive cell, E_{Si} , E_V , E_{Ge} , and E_N is the energy per atom of Si, V, Ge and N in their most stable phases, respectively, and n is the number of atoms in the primitive cell. The calculated value of E_f is about -0.602 eV/atom, implying that ML VSiGeN₄ has a good thermodynamical stability against the elemental phases. Therefore, we expect that ML VSiGeN₄ can be synthesized experimentally, for example by substituting atoms in ML MoSi₂N₄ [45].

Next, the magnetic properties of ML VSiGeN₄ is investigated. We calculate the total energies of different magnetic states: ferromagnetic (FM), nonmagnetic (NM), antiferromagnetic (AFM1 and 120° AFM) structures, which are shown in Fig. S1. The results show that the total energy of FM structure is the lowest, 76 meV per unit cell lower than the AFM1 state, 351 meV per unit cell lower than NM state. Besides, the spin configuration of 120° AFM is unstable and transforms into FM state, which is similar to 2H-VSSe and LaBrI [30, 46]. Thus, FM state is the ground state, which can be interpreted by the Goodenough-Kanamori-Anderson (GKA) rules [47–50]. In ML VSiGeN₄, the V-N-V bonding angle is 91.8°, close to 90°. According to the GKA rules, such a structure configuration favors FM coupling. To determine the easy magnetization axis, we calculated magnetic anisotropy energy (MAE), which is defined as $E_M = E_{[100]} - E_{[001]}$, where $E_{[100]}$ and $E_{[001]}$ represent the total energy of system with the spin orientation of V atoms along out-of-plane and in-plane, respectively. The E_M is 72 μ eV per unit cell, which means that ML VSiGeN₄ is out-of-plane magnetization. Such magnetization direction is necessary to realize the spontaneous valley polarization.

To study the magnetic stability of ML VSiGeN₄, we estimated the Curie temperature (T_C) by using the classical Metropolis MC simulations based on the Heisenberg model: $H = -\sum_{\langle ij \rangle} J_{ij} S_i \cdot S_j - D(S_{iz})^2$. Where S_i is the normalized spin vector on site i , J_{ij} is the exchange interaction strength between sites i and j , D is the single-site MAE, S_{iz} represents component of S along z orientation, and $|S| = \frac{1}{2}$ for V in 2D VSiGeN₄. Because the moment of the V atom is around 1 μ_B . With $J = 51.49$ meV and $D = 72 \mu$ eV, the result of MC simulation shows that the value of T_C is about 113 K (Fig. S1(d)), which is much higher than CrI₃ (45 K) and Cr₂Ge₂Te₆ bilayer (30 K) [51, 52].

IV. ELECTRONIC STRUCTURES AND STRAIN-DRIVEN VALLEY STATES

The spin polarized band structure of the ML VSiGeN₄ without considering SOC is shown in Fig. 2(a). It can be seen that spin-down and spin-up channels split significantly, and there is only spin-up states around the Fermi level (E_F). The material is a semiconductor with a small direct band gap of

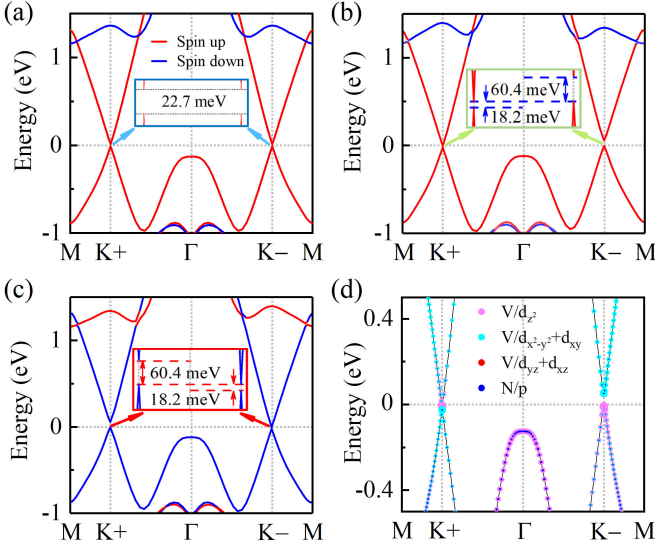


FIG. 2. The spin polarized band structures of ML VSIGeN₄ (a) without SOC; (b) and (c) with SOC for magnetic moment of V along the positive and negative z direction, respectively. (d) Orbital-resolved spin polarized band structure with SOC in ML material. Spin projections along the out-of-plane direction are indicated by red (positive direction, spin-up) and blue (negative direction, spin-down) line for VSIGeN₄ in (b) and (c).

22.7 meV. Both the valence band maximum (VBM) and the conduction band minimum (CBM) locate at the high symmetry point K. The degenerate valleys at the K+ and K- point are nonequivalent due to the break of the inversion symmetry. Therefore, ML VSIGeN₄ is a valleytronic material. Similar to the previously reported ferrovalley materials, when considering both SOC and magnetic exchange interaction, ML VSIGeN₄ spontaneously enables a valley polarization without any additional tuning. As shown in Fig. 2(b), the SOC lifts the energy degeneracy of K+ and K- valley (the energy of K- valley is higher than K+ valley for both valence band and conduction band) with valley polarization of 60.4 meV (18.2 meV) at conduction (valence) band. This polarization value is larger than previously those of reported materials, such as VSIGeP₄ (49.4 meV) [25], LaBr₂ (33 meV) [29], Cr₂Se₃ (18.7 meV) [26] and TiVI₆ (22 meV) [38]. More importantly, the influence of irrelevant bands for valley properties is minimum in the energy range of (-0.2 ~ 1 eV). The linear band dispersion around K- and K+ valley show a high Fermi velocity of about $0.31 \times 10^6 \text{ m s}^{-1}$, which has the same order of magnitude as graphene. The valley polarization can be tuned by an external magnetic field. As shown in Fig. 2(c), the valley polarization and spin state are flipped by reversing the magnetization of V atoms, so that all K valley states now occupy the spin-down channel and K- valley state has a lower energy than K+ valley. The tunable large valley polarization, large Fermi velocity, and the clean single spin state around E_F , endow VSIGeN₄ with more advantages than most valleytronics materials in practical applications.

The different values of valley polarization between K+ and K- valley can be attributed to the different orbital contribu-

tions. As shown in Fig. 2(d), at K+ valley, the CBM is contributed by d_{z^2} orbital of V and the VBM is contributed by $d_{x^2-y^2} + d_{xy}$ orbital of V, while the situation at K- valley is reversed. Since the magnetic quantum number (m_z) of d_{z^2} orbital is 0, the basis functions composed of this orbital is the same at K+ and the K- point. While basis functions composed of $d_{x^2-y^2}$ and d_{xy} orbital is different at K+ and the K- point, which can be chosen as: $|\psi\rangle = \frac{1}{\sqrt{2}}(|d_{x^2+y^2}\rangle + i\tau|d_{xy}\rangle)$. Here $\tau = \pm 1$ indicates the valley index at the K \pm point [25]. Therefore, introducing SOC into a system with neither time-reversal symmetry nor space-reversal symmetry will result in different energy eigenvalues at K+ point and K- point with different basis functions, leading to the occurrence of valley polarization.

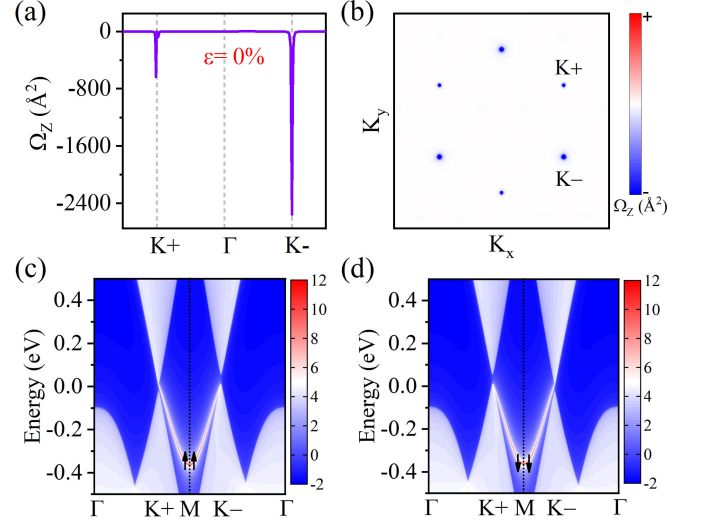


FIG. 3. (a) and (b) The distribution of Berry curvature along the high symmetry path and along the whole BZ in strain-free ML VSIGeN₄, respectively. (c) and (d) The edge state for ML VSIGeN₄ with magnetic moment along positive and negative z direction, respectively.

The opposite orbital order for the K- and K+ valleys imply that ML VSIGeN₄ has topological properties, such as VQAHE effect. This anomalous transport phenomenon is related to the Berry curvature $\Omega(k)$. For a 2D systems, $\Omega(k)$ only has z component $\Omega_z(k)$. It can be calculated by [53]:

$$\Omega_z(k) = - \sum_n \sum_{n' \neq n} f_n \frac{2Im\langle\psi_{nk}|v_x|\psi_{n'k}\rangle\langle\psi_{n'k}|v_y|\psi_{nk}\rangle}{(E_n - E_{n'})^2},$$

where n and n' are band indexes; f_n is the equilibrium Fermi-Dirac distribution function for the n -th band at a k point; $v_x(y)$ is the velocity operator along the $x(y)$ direction; k is the wave vector; ψ_{nk} is the Bloch wave function with eigenvalue E_n and $E_{n'}$.

In Fig. 3(a) and Fig. 3(b), we show the $\Omega_z(k)$ distribution of ML VSIGeN₄ along the high symmetry path and contour map in the 2D Brillouin zone (BZ), respectively. One clearly observes that the values of $\Omega_z(k)$ are all zero except the region around K+ and K- valleys. More importantly, the sign is same and the magnitudes are different from two valleys. With such distribution of $\Omega_z(k)$, the material may have a

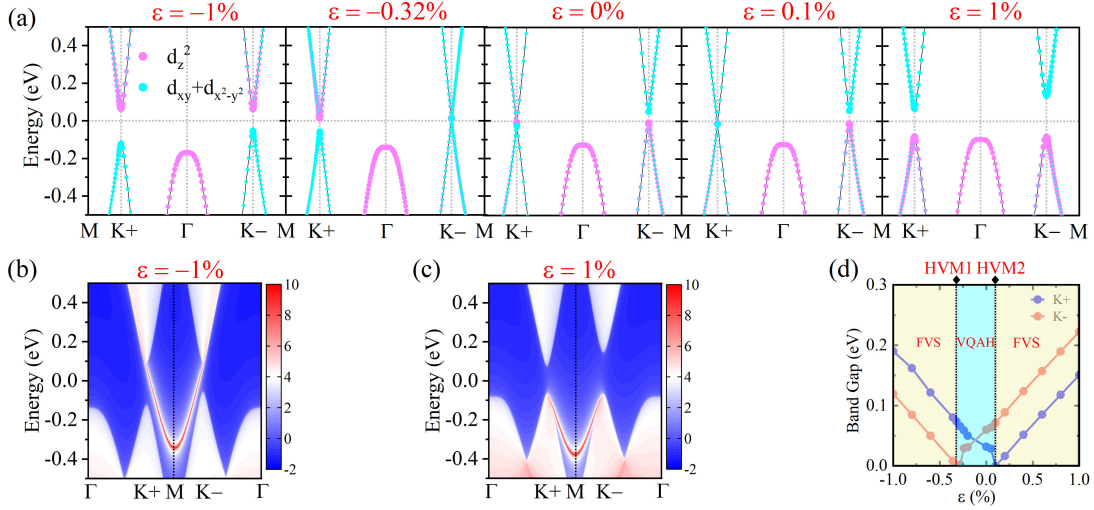


FIG. 4. (a) The evolution of orbital-projected band with SOC under different biaxial strain, respectively. (b) and (c) The edge state for ML VSIGeN₄ under $\varepsilon = -1\%$ and $\varepsilon = 1\%$, respectively. (d) The diagram of topological phase transitions and the variation of the band gaps at K valley with different strain.

nonzero Chern number and edge states protected by the non-trivial topological property, which result in a VQAH effect. We have evaluated the Chern number (C) of ML VSIGeN₄ via formula: $C = \frac{1}{2\pi} \int_{BZ} d^2k \Omega_z(k)$. The result shows that the Chern number is 1. Then, we calculated the edge states as shown in Fig. 3(c), it can be seen that a topological nontrivial chiral edge state connecting conduction bands (K+ valley) and valence bands (K- valley) is clearly visible. Due to CBM and VBM all dominated by spin-up states, the edge state is also spin-up with 100% spin polarization. Similar to the reversal of valley polarization under external magnetic field, when the magnetization of V is reversed, the edge state will change accordingly. As shown in Fig. 3(d), it becomes spin-down state and connect conduction bands (K+ valley) and valence bands (K- valley) with opposite chiral. Besides, the conductive edge state of spin-up in the global band gap mainly locate at K+ valley, the location of edge state change from K+ valley to K- valley when spin flipping, which revealed a behavior of the chiral-spin-valley locking for the edge state [32]. Thus, above properties indicate that ML VSIGeN₄ features an intrinsically VQAH effect.

The electronic properties of low-dimensional materials can be generally tuned by strain [54–59]. Here, we introduce biaxial strain in ML VSIGeN₄ and study the effect of strain on the band structure. The biaxial strain strength is defined as $\varepsilon = \frac{b-b_0}{b_0}$, where b and b_0 are the strained and unstrained lattice constant, respectively. The result is shown in Fig. 4(a) and Fig. S2. It shows that the band gap is obviously changed under different strain. Specially, when $\varepsilon = -0.32\%$ or 0.1% , the material transforms into HVM state with 100% valley polarization and 100% spin polarization. In such a state, one valley is metallic and the other one is semiconductor with same spin-up state. The gapless valley shows a Dirac cone-like linear dispersion with a Fermi velocity of $3.58 \times 10^5 \text{ m s}^{-1}$. Changing the strain can open a gap, and the HVM state is thus disappeared. As the strain increases, the band gap of the two

valleys also increases gradually, whereas the large valley polarization always remains (see Fig. 4(d)). Specially, the valley polarization only appears at valence band for -1% strained VSIGeN₄, while in the case of 1% strain, only the conduction band has different energy for K+ and K- valley. This phenomenon also originates from the change of orbital composition, as discussed earlier. Only $d_{x^2-y^2} + d_{xy}$ orbital has different energy eigenvalues at different valley, and this orbital constitute the valence band for $\varepsilon = -1\%$ and the conduction band for $\varepsilon = 1\%$, respectively. Thus, leading to different valley polarization behaviors.

As shown in Fig. 4(a), from $\varepsilon = -1\%$ to $\varepsilon = 1\%$, the orbital composition of the band at two valleys is reversed. This band inversion occurs sequentially in the K- ($\varepsilon = -0.32\%$) and K+ valleys ($\varepsilon = 0.1\%$) via two HVM states, implying the occurrence of topological phase transition. We calculated edge state of the material under $\varepsilon = \pm 1\%$, respectively. As shown in Fig. 4(b) and Fig. 4(c), one clearly observes that an edge state connecting conduction bands ($\varepsilon = -1\%$) or valence bands ($\varepsilon = 1\%$). Therefore, the system transforms from topological nontrivial state (VQAH state) to trivial state (FVS) under strain. In order to understand the division of different phases more intuitively, we plot a phase diagram with the variation of the band gaps at two valleys for ML VSIGeN₄. As shown in Fig. 4(d), the band gaps change linearly with strain at two valleys, and the band gap at each valley has a process of closing and reopening, where the gapless states in the process correspond to the two HVM states. During this process, a topological phase transition from VQAH state to FVS occurs. Therefore, small strain can induce phase transition and effectively tune the electronic structure along with the valley state. Besides, we also calculated energy difference between different magnetic states under strain (Fig. S3), which reveal that FM state is still the ground state under different strain.

For FVS systems, there exist nonzero Berry curvature with different values at K+ and K- valley. As shown in Fig. 5(a)

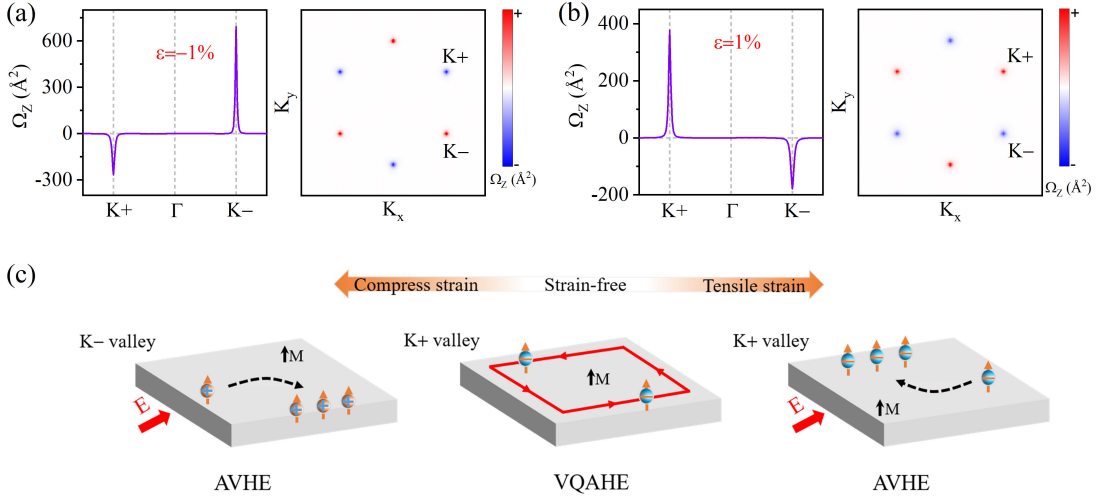


FIG. 5. (a) and (b) The distribution of Berry curvature along the high symmetry path and along the whole BZ under $\varepsilon = -1\%$ and $\varepsilon = 1\%$, respectively. (c) Schematic diagram of multiple valley Hall effect in ML VSiGeN₄ tuned by strain. The holes and electrons are denoted by blue + and orange - symbol, respectively. Upward arrows in orange color refer to the spin-up carriers. Red frame represents edge state.

and Fig. 5(b), when $\varepsilon = -1\%$, the $\Omega_z(k)$ have different magnitudes with opposite signs at two valleys, which revealing the typical valley contrasting characteristic in ML VSiGeN₄. Due to the topological phase transition, both the sign and magnitude of $\Omega_z(k)$ are modified (see Fig. 3(a)). So, when $\varepsilon = 1\%$, the sign of $\Omega_z(k)$ at K+ and K- valley is opposite to the case of $\varepsilon = -1\%$. As a result, the sign and magnitude of $\Omega_z(k)$ for different valleys can be changed by applying a small strain. The tunable sign of Berry curvature has been reported by reversing ferroelectric polarization and magnetization [24, 37]. Here, we propose a convenient method to modulate the Berry curvature.

With a nonzero $\Omega_z(k)$, the electrons will acquire an anomalous transverse velocity $v_n(k)$ under an in-plane longitudinal electric field E , where $v_n(k) = \frac{\partial \varepsilon_n(k)}{\hbar \partial k} - \frac{e}{\hbar} E \times \Omega_n(k)$ [60], and induce AVHE. Fig. 5(c) displays multiple valley Hall effects in ML VSiGeN₄ which can be tuned by applying strain. For strain-free ML VSiGeN₄, the VQAHE with one spin-polarized edge state can be presented. The edge state is chiral-spin-valley locking, which means that when the magnetization direction is reversed, the chiral, spin, and valley of the edge state will also flip. For FVS state under compressive strain (larger than -0.32%), when shifting the Fermi level between the K+ and K- valleys in the valence band (Fig. 4 and Fig. S2), the spin-up holes at K- valley flow to right side of the sample under an external in-plane electric field E , thus the AVHE occurs. For FVS state under tensile strain (larger than 0.1%), valley polarization occurs at conduction band. In this case, the spin-up electrons from the K+ valley accumulated at the left side of the sample under electric field E . With spin-up carriers are only accumulated at one side of the sample, the Hall voltage can be detected. Besides, when reverse the magnetization orientation, the conductive valley is changed (from K+(K-) valley to K-(K+) valley), and because of the spin flipping, the direction of the lateral movement of the carriers changes accordingly, and thus the sign of Hall voltage

changes. Therefore, the valley degree of freedom can be selectively manipulated in ML VSiGeN₄ by applying strain and magnetic field.

Except for valley-related Hall effect, the different polarized light absorption is also an important topic of valleytronics and valley physics. The chirality of different valleys in the same material is usually different, and one chirality corresponds to one polarized light absorption. The change in sign of $\Omega_z(k)$ under strain implies the change in valley chirality. We calculated valley-selective circular dichroism of ML VSiGeN₄ under different strain as displayed in Fig. 6. The degree of circular polarization $\eta(k) = \frac{|M_+(k)|^2 - |M_-(k)|^2}{|M_+(k)|^2 + |M_-(k)|^2}$ [8] indicates the difference between the absorption of right-handed and left-handed polarized lights (σ_{\pm}) at each k point, and $M_{\pm}(k)$ is the transition matrix of circular polarization. One clearly observes that both the K \pm valleys mainly absorbs σ_- in strain-free ML VSiGeN₄. This selective absorption of polarized light can be used in optoelectronic devices such as filter. For two HVM states, the material still mainly absorbs σ_- , but only one of the two valleys has light absorption because the other valley is gapless. Differently, the absorption occurs at K+ valley for HVM1 state ($\varepsilon = -0.32\%$) and K- valley for HVM2 state ($\varepsilon = 0.1\%$). Under a larger strain, the phase transition will occur, and the valley chirality will change. As shown in Fig. 6, when $\varepsilon = \pm 1\%$, the two valleys absorb different polarized lights, and for a particular valley, opposite polarized light is absorbed under tensile and compressive strain. As a result, strain can also induce change of valley chirality, enabling the manipulation of polarized light absorption at different valleys.

V. CONCLUSIONS

In summary, combining first principles calculations with Wannier-function-based tight-binding model, we demonstrate the structural stability, ferromagnetism, valley-dependent

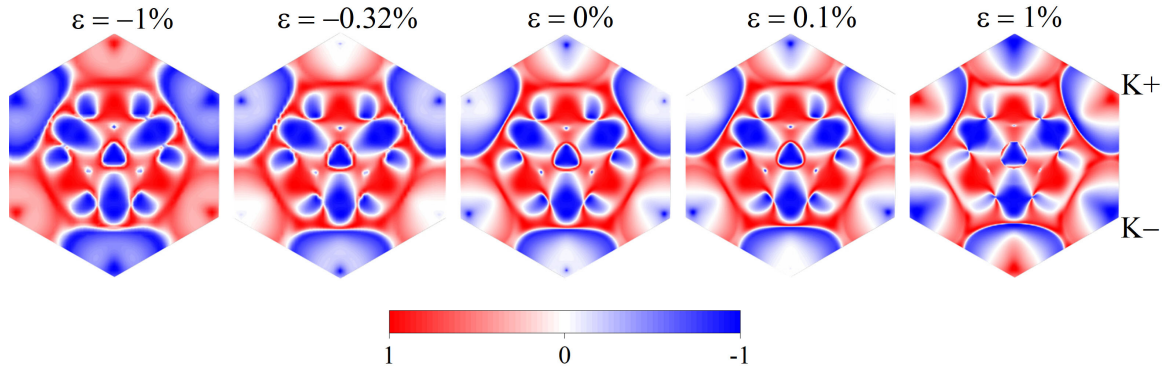


FIG. 6. The BZ colour-coded by the degree of circular polarization $\eta(k)$ of MLVSiGeN₄ under different strain, respectively. ± 1 representative completely absorption left- (σ_+) and right-handed (σ_-) polarized light, respectively.

properties, topological properties and strain-induced phase transition of ML VSiGeN₄. The results show that ML VSiGeN₄ is a ferromagnetic semiconductor with out-of-plane magnetization and a T_C of 113 K. Simultaneously, it intrinsically exhibits a VQAHE with 100% spin polarization edge state and spontaneous valley polarization. By applying tensile strain of 0.1% and compressive strain of 0.32%, the HVM state with 100% valley polarization can be acquired. The FVS state can be achieved by further increasing the strain, and it has an AVHE that can be modulated by flipping the magnetization direction. The strain-tunable polarized light absorption at different valleys can be applied to the next generation photoelectric device. Our work provides a good material platform for the interplay between valleytronics, spintronics, and topology.

ACKNOWLEDGMENTS

This work was financially supported by the National Natural Science Foundation of China (No. 11904079, No. 12104130, No. 12047517), the Natural Science Foundation of Henan (No. 202300410069), the China Postdoctoral Science Foundation (No. 2020M682274, No. 2020TQ0089) and the Foundation of Henan Educational Committee (No. 22A140015). Thanks to Dr. Shan Guan from Institute of Semiconductors in Chinese Academy of Sciences and Dr. Botao Fu from College of Physics and Electronic Engineering in Sichuan Normal University for their helpful discussions. The authors acknowledge Beijing PARATERA Tech CO.,Ltd. for providing HPC resources that have contributed to the research results reported within this paper.

-
- [1] O. Gunawan, Y. P. Shkolnikov, K. Vakili, T. Gokmen, E. P. De Poortere, and M. Shayegan, "Valley susceptibility of an interacting two-dimensional electron system," *Phys. Rev. Lett.* **97**, 186404 (2006).
 - [2] D. Xiao, W. Yao, and Q. Niu, "Valley-contrasting physics in graphene: Magnetic moment and topological transport," *Phys. Rev. Lett.* **99**, 236809 (2007).
 - [3] J. Schaibley, H. Yu, G. Clark, P. Rivera, J. Ross, K. Seyler, W. Yao, and X. Xu, "Valleytronics in 2D materials," *Nat. Rev. Mater.* **1**, 16055 (2016).
 - [4] A. Rycerz, J. Worzydo, and C. W. J. Beenakker, "Valley filter and valley valve in graphene," *Nat. Phys.* **3**, 172 (2007).
 - [5] G. Aivazian, Z. Gong, A. Jones, R.L. Chu, J. Yan, D. G. Mandrus, C. Zhang, D. Cobden, W. Yao, and X. Xu, "Magnetic control of valley pseudospin in monolayer WSe₂," *Nat. Phys.* **11**, 148 (2014).
 - [6] H. Zeng, J. Dai, W. Yao, D. Xiao, and X. Cui, "Valley polarization in MoS₂ monolayers by optical pumping," *Nat. Nanotechnol.* **7**, 490 (2012).
 - [7] K. Mak, K. He, J. Shan, and T. Heinz, "Control of valley polarization in monolayer MoS₂ by optical helicity," *Nat. Nanotechnol.* **7**, 494 (2012).
 - [8] T. Cao, G. Wang, W. Han, H. Ye, C. Zhu, J. Shi, Q. Niu, P. Tan, E. Wang, B. Liu, and J. Feng, "Valley-selective circular dichroism of monolayer molybdenum disulphide," *Nat. Commun.* **3**, 887 (2012).
 - [9] D. Xiao, G.B. Liu, W. Feng, X. Xu, and W. Yao, "Coupled spin and valley physics in monolayers of MoS₂ and other group-vi dichalcogenides," *Phys. Rev. Lett.* **108**, 196802 (2012).
 - [10] S. Wu, J. Ross, G.B. Liu, G. Aivazian, A. Jones, Z. Fei, W. Zhu, D. Xiao, W. Yao, D. Cobden, and X. Xu, "Electrical tuning of valley magnetic moment through symmetry control in bilayer MoS₂," *Nature Phys.* **9**, 149 (2013).
 - [11] Y. Li, J. Ludwig, T. Low, A. Chernikov, X. Cui, G. Arefe, Y. Kim, A. van der Zande, A. Rigosi, H. M. Hill, S. H. Kim, J. Hone, Z. Li, D. Smirnov, and T. F. Heinz, "Valley splitting and polarization by the zeeman effect in monolayer MoSe₂," *Phys. Rev. Lett.* **113**, 266804 (2014).
 - [12] D. MacNeill, C. Heikes, K. Mak, Z. Anderson, A. Kormányos, V. Zólyomi, J. Park, and D. Ralph, "Breaking of valley degeneracy by magnetic field in monolayer MoSe₂," *Phys. Rev. Lett.* **114**, 037401 (2015).
 - [13] A. Srivastava, M. Sidler, A. Allain, D. Lembke, A. Kis, and A. Imamolu, "Valley zeeman effect in elementary optical excitations of monolayer WSe₂," *Nat. Phys.* **11**, 141 (2015).
 - [14] G. Sallen, L. Bouet, X. Marie, G. Wang, C. R. Zhu, W. P. Han, Y. Lu, P. H. Tan, T. Amand, B. L. Liu, and B. Urbaszek, "Robust optical emission polarization in MoS₂ monolayers through selective valley excitation," *Phys. Rev. B* **86**, 081301 (2012).

- [15] G. Kioseoglou, A. T. Hanbicki, M. Currie, A. L. Friedman, D. Gunlycke, and B. T. Jonker, "Valley polarization and intervalley scattering in monolayer MoS_2 ," *Appl. Phys. Lett.* **101**, 221907 (2012).
- [16] S. Guan, G. Zhang, and C. Liu, "Enhanced in-plane ferroelectricity, antiferroelectricity, and unconventional 2D emergent fermions in quadruple-layer XSbO_2 ($X = \text{Li}, \text{Na}$)," *Nanoscale* **13**, 19172 (2021).
- [17] S. Guan and J. W. Luo, "Electrically switchable hidden spin polarization in antiferroelectric crystals," *Phys. Rev. B* **102**, 184104 (2020).
- [18] F. Withers, O. Del Pozo-Zamudio, A. Mishchenko, A. P. Rooney, A. Gholinia, K. Watanabe, T. Taniguchi, S. J. Haigh, A. K. Geim, A. I. Tartakovskii, and K. S. Novoselov, "Light-emitting diodes by band-structure engineering in van der waals heterostructures," *Nat. Mater.* **14**, 301 (2015).
- [19] C. H. Lee, G. Hy. Lee, A. van der Zande, W. Chen, Y. Li, M. Han, X. Cui, G. Arefe, C. Nuckolls, T. Heinz, J. Guo, J. Hone, and P. Kim, "Atomically thin pn junctions with van der waals heterointerfaces," *Nat. Nanotechnol.* **9**, 676 (2014).
- [20] L. Xu, M. Yang, L. Shen, J. Zhou, T. Zhu, and Y. Feng, "Large valley splitting in monolayer WS_2 by proximity coupling to an insulating antiferromagnetic substrate," *Phys. Rev. B* **97**, 041405 (2018).
- [21] T. Norden, C. Zhao, P. Zhang, R. Sabirianov, A. Petrou, and H. Zeng, "Giant valley splitting in monolayer WS_2 by magnetic proximity effect," *Nat. Commun.* **10**, 4163 (2019).
- [22] R. Peng, Y. Ma, S. Zhang, B. Huang, and Y. Dai, "Valley polarization in janus single-layer MoSSe via magnetic doping," *J. Phys. Chem. Lett.* **9**, 3612 (2018).
- [23] J. Qi, X. Li, Q. Niu, and J. Feng, "Giant and tunable valley degeneracy splitting in MoTe_2 ," *Phys. Rev. B* **92**, 121403 (2015).
- [24] W. Y. Tong, S. J. Gong, X. Wan, and C. G. Duan, "Concepts of ferrovalley material and anomalous valley hall effect," *Nat. Commun.* **7**, 13612 (2016).
- [25] X. Feng, X. Xu, Z. He, R. Peng, Y. Dai, B. Huang, and Y. Ma, "Valley-related multiple hall effect in monolayer VSi_2P_4 ," *Phys. Rev. B* **104**, 075421 (2021).
- [26] Z. He, R. Peng, X. Feng, X. Xu, Y. Dai, B. Huang, and Y. Ma, "Two-dimensional valleytronic semiconductor with spontaneous spin and valley polarization in single-layer Cr_2Se_3 ," *Phys. Rev. B* **104**, 075105 (2021).
- [27] H. X. Cheng, J. Zhou, W. Ji, Y. N. Zhang, and Y. P. Feng, "Two-dimensional intrinsic ferrovalley GdI_2 with large valley polarization," *Phys. Rev. B* **103**, 125121 (2021).
- [28] Q. Cui, Y. Zhu, J. Liang, P. Cui, and H. Yang, "Spin-valley coupling in a two-dimensional VSi_2N_4 monolayer," *Phys. Rev. B* **103**, 085421 (2021).
- [29] P. Zhao, Y. Ma, C. Lei, H. Wang, B. Huang, and Y. Dai, "Single-layer LaBr_2 : Two-dimensional valleytronic semiconductor with spontaneous spin and valley polarizations," *Appl. Phys. Lett.* **115**, 261605 (2019).
- [30] P. Jiang, L. Kang, Y. L. Li, X. Zheng, Z. Zeng, and S. Sanvito, "Prediction of the two-dimensional janus ferrovalley material LaBrI ," *Phys. Rev. B* **104**, 035430 (2021).
- [31] S. D. Guo, J. X. Zhu, W. Q. Mu, and B. G. Liu, "Possible way to achieve anomalous valley hall effect by piezoelectric effect in a GdCl_2 monolayer," *Phys. Rev. B* **104**, 224428 (2021).
- [32] H. Huan, Y. Xue, B. Zhao, G. Gao, H. Bao, and Z. Yang, "Strain-induced half-valley metals and topological phase transitions in MBr_2 monolayers ($M = \text{Ru}, \text{Os}$)," *Phys. Rev. B* **104**, 165427 (2021).
- [33] Y. Zang, Y. Ma, R. Peng, H. Wang, B. Huang, and Y. Dai, "Large valley-polarized state in single-layer NbX_2 ($X = \text{S}, \text{Se}$): Theoretical prediction," *Nano Res.* **14**, 934 (2021).
- [34] S. Li, Q. Wang, C. Zhang, P. Guo, and S. A. Yang, "Correlation-driven topological and valley states in monolayer VSi_2P_4 ," *Phys. Rev. B* **104**, 085149 (2021).
- [35] H. Hu, W. Tong, Y. Shen, X. Wan, and C. G. Duan, "Concepts of the half-valley-metal and quantum anomalous valley hall effect," *npj Quantum Mater.* **6**, 129 (2020).
- [36] Yi. F. Zhao, Y. H. Shen, H. Hu, W. Y. Tong, and C. G. Duan, "Combined piezoelectricity and ferrovalley properties in janus monolayer VClBr ," *Phys. Rev. B* **103**, 115124 (2021).
- [37] X. Liu, A. Pyatakov, and W. Ren, "Magnetoelectric coupling in multiferroic bilayer VS_2 ," *Phys. Rev. Lett.* **125**, 247601 (2020).
- [38] W. Du, Y. Ma, R. Peng, H. Wang, B. Huang, and Y. Dai, "Prediction of single-layer TiVl_6 as a promising two-dimensional valleytronic semiconductor with spontaneous valley polarization," *J. Mater. Chem. C* **8**, 13220 (2020).
- [39] J. Liu, W. J. Hou, C. Cheng, H. X. Fu, J. T. Sun, and S. Meng, "Intrinsic valley polarization of magnetic VSe_2 monolayers," *Journal of Physics: Condensed Matter* **29**, 255501 (2017).
- [40] P. E. Blöchl, "Projector augmented-wave method," *Phys. Rev. B* **50**, 17953 (1994).
- [41] G. Kresse and J. Furthmüller, "Efficient iterative schemes for ab initio total-energy calculations using a plane-wave basis set," *Phys. Rev. B* **54**, 11169 (1996).
- [42] J. Perdew, K. Burke, and M. Ernzerhof, "Generalized gradient approximation made simple," *Phys. Rev. Lett.* **77**, 3865–3868 (1996).
- [43] G. Pizzi, V. Vitale, R. Arita, S. Blgel, F. Freimuth, G. Granton, M. Gibertini, D. Gresch, C. Johnson, T. Koretsune, J. Ibaez-Azpiroz, H. Lee, J.-M. Lihm, D. Marchand, A. Marrazzo, Y. Mokrousov, J. I. Mustafa, Y. Nohara, Y. Nomura, and L. Paulatto et al., "Wannier90 as a community code: new features and applications," *J. Physics.: Condens. Matter* **32**, 165902 (2020).
- [44] Q. Wu, S. Zhang, H. F. Song, M. Troyer, and A. Soluyanov, "WannierTools: An open-source software package for novel topological materials," *Comput. Phys. Commun.* **224**, 405–416 (2018).
- [45] Y. L. Hong, Z. Liu, L. Wang, T. Zhou, W. Ma, C. Xu, S. Feng, L. Chen, M. L. Chen, D. M. Sun, X. Q. Chen, H. M. Cheng, and W. Ren, "Chemical vapor deposition of layered two-dimensional MoSi_2N_4 materials," *Science* **369**, 670 (2020).
- [46] C. Zhang, Y. Nie, S. Sanvito, and A. Du, "First-principles prediction of a room-temperature ferromagnetic janus VSSe monolayer with piezoelectricity, ferroelasticity, and large valley polarization," *Nano Lett.* **19**, 1366 (2019).
- [47] Y. Wu, W. Sun, S. Liu, B. Wang, C. Liu, H. Yin, and Z. Cheng, " $\text{Ni}(\text{NCS})_2$ monolayer: a robust bipolar magnetic semiconductor," *Nanoscale* **13**, 16564 (2021).
- [48] John B. Goodenough, "Theory of the role of covalence in the perovskite-type manganites $[\text{La}, \text{M}(\text{II})]\text{MnO}_3$," *Phys. Rev.* **100**, 564 (1955).
- [49] P. W. Anderson, "New approach to the theory of superexchange interactions," *Phys. Rev.* **115**, 2 (1959).
- [50] J. Kanamori, "Crystal distortion in magnetic compounds," *J. Appl. Phys.* **31**, S14 (1960).
- [51] B. Huang, G. Clark, E. Navarro-Moratall, D. Klein, R. Cheng, K. Seyler, D. Zhong, E. Schmidgall, M. McGuire, D. Cobden, P. Jarillo-Herrero W. Yao, D. Xiao, and X. Xu, "Layer-dependent ferromagnetism in a van der waals crystal down to the monolayer limit," *Nature* **546**, 270 (2017).
- [52] C. Gong, L. Li, Z. Li, H. Ji, A. Stern, Y. Xia, T. Cao, W. Bao, C. Wang, Y. Wang, Z. Q. Qiu, R. J. Cava, S. Louie, J. Xia,

- and X. Zhang, “Discovery of intrinsic ferromagnetism in two-dimensional van der waals crystals,” *Nature* **546**, 265 (2017).
- [53] S. Li, W. Wu, X. Feng, S. Guan, W. Feng, Y. Yao, and S. A. Yang, “Valley-dependent properties of monolayer MoSi_2N_4 , WSi_2N_4 , and MoSi_2As_4 ,” *Phys. Rev. B* **102**, 235435 (2020).
- [54] S. Guan, Z. M. Yu, Y. Liu, G. B. Liu, L. Dong, Y. Lu, and Y. Yao, “Artificial gravity field, astrophysical analogues, and topological phase transitions in strained topological semimetals,” *npj Quantum Mater.* **2**, 23 (2017).
- [55] C. Liu, B. Fu, H. Yin, G. Zhang, and C. Dong, “Strain-tunable magnetism and nodal loops in monolayer MnB ,” *Appl. Phys. Lett.* **117**, 103101 (2020).
- [56] C. Liu, S. Guan, H. Yin, W. Wan, Y. Wang, and Y. Zhang, “ γ – GeSe : A two-dimensional ferroelectric material with doping-induced ferromagnetism,” *Appl. Phys. Lett.* **115**, 252904 (2019).
- [57] P. Liu, G. Zhang, Y. Yan, G. Jia, C. Liu, B. Wang, and H. Yin, “Strain-tunable phase transition and doping-induced magnetism in iodine,” *Appl. Phys. Lett.* **119**, 102403 (2021).
- [58] C. Liu, B. Wang, G. Jia, P. Liu, H. Yin, S. Guan, and Z. Cheng, “Tunable magnetism in ferroelectric α – In_2Se_3 by hole-doping,” *Appl. Phys. Lett.* **118**, 072902 (2021).
- [59] S. Liu, H. Yin, D. J. Singh, and P. F. Liu, “ Ta_4SiTe_4 : A possible one-dimensional topological insulator,” *Phys. Rev. B* **105**, 195419 (2022).
- [60] D. Xiao, M. C. Chang, and Q. Niu, “Berry phase effects on electronic properties,” *Rev. Mod. Phys.* **82**, 1959 (2010).